Rev. Roum. Sci. Techn.– Électrotechn. et Énerg.
Vol. **68**, *2*, pp. 194–199, Bucarest, 2023

WIRELESS POWER TRANSFER FOR UNDERWATER VEHICLES

ALI AGCAL[1], ALTAN KALAY[2], RAMAZAN CETIN[3]

Keywords: Wireless power transfer; Underwater vehicle; Inductive coupling; Eddy current loss.

Wireless power transfer (WPT) through magnetic resonance coupling (MRC) offers a safe and simple solution for underwater (UV) vehicles without being affected by water conductivity. Due to its ease of control in WPT systems, the most suitable topology is Serial-Serial (SS). In this study, square transmitting and receiving coils with dimensions of 40 cm - 40 cm were designed for 3.3 kW power transmission at 85 kHz. The design was studied in the air, pure water, and seawater environments. Three different cases were analyzed with ANSYS Maxwell 3D. The WPT system responded similarly in air and pure water environments. However, it was determined that the eddy current loss increased, the mutual inductance decreased, the coupling factor weakened, and the critical air gap decreased by about 0.2 cm in the seawater environment. The results showed that the WPT system's efficiency was similar for air and pure water but tolerably lower in the marine environment. Further, the health effects of the WPT design were examined through the ANSYS HFSS, in line with the IEEE standard and ICNIRP guidelines.

1. INTRODUCTION

Today, many internal combustion technologies have been replaced by more efficient electrical systems. This development has increased the need for electrical energy and energy demand, especially for battery systems. Battery-operated systems such as electric vehicles, crewless aerial vehicles, drones, and underwater vehicles (UV) have constantly become in need of energy due to the insufficient energy density of batteries. With WPT, the charging continuity of UV can be achieved autonomously without human control [1]. In the charging of UV, even a tiny insulation problem in cable systems can cause significant problems since the corrosiveness and conductivity of seawater is high. These problems can be minimized with the WPT system. The WPT system will occupy an essential place in the future due to its electrical isolation and reliability.

According to the literature, WPT can be achieved through various methods, including microwave, laser, capacitive coupling, and inductive coupling [2]. Any of these WPT technologies can be used depending on the application area. Wireless charging of UV is done in the near field [3]. Magnetic resonance coupling theory is the most efficient and convenient method in the near field [4]. In magnetic resonance coupling theory, energy is transferred from transmitter to receiver via magnetic coupling. In addition, using the resonance structure ensures the transfer is carried out efficiently. The WPT system for UV is shown in Fig 1.

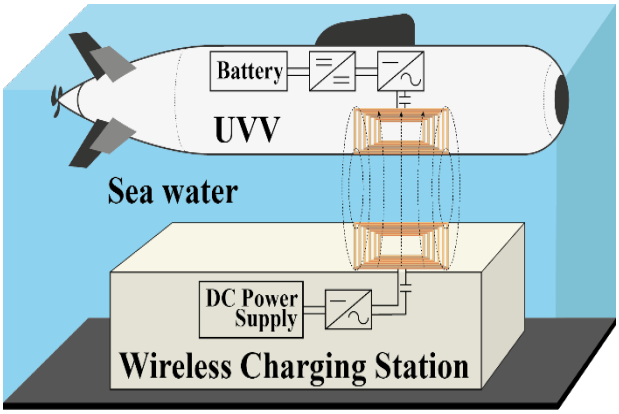

Fig. 1 – Submarine Vehicle Charging System

The efficient energy transmission depends on the frequency, the coil size, the distance between the coils, and the material between the coils [5]. Therefore, the design of the WPT system is calculated by considering these parameters. There are various topologies in the WPT system. These topologies are shaped by how the capacitor is connected to the circuit. Among the basic WPT topologies, the serial-serial (SS) topology is highly efficient and can operate in a wide load range [6]. For this reason, the SS topology will be used to perform wireless charging among the four basic topologies.

Many designs are related to UV wireless charging in the literature [7]. Magnetic resonance coupling theory-based systems are mainly used for UV wireless charging. In addition, studies are carried out with UV capacitive coupling [8, 9]. The capacitively coupled WPT system is not a very suitable topology for marine water systems with high conductivity. In the WPT system with inductive coupling, losses occur, albeit low, due to eddy currents. The current and operating frequency effect on eddy current loss was analyzed [5]. A new coil structure has been developed with a multi-transmitter design to reduce the eddy currents generated in the wireless charging of UV vehicles [10]. Autonomous UV's wireless energy and data transmission have been studied [11]. An arc-shaped coil design suitable for the curved shell of the autonomous UV has been studied [12]. A three-phase wireless charging system was proposed for the light autonomous UV [13]. The misalignment tolerance and transmission performance in wireless charging of UV vehicles is significantly improved by designing a new hybrid transmitter consisting of conical and planar spiral coils [14].

This study designed a wireless charging system for UV by underwater placing a transmitter and receiver coil. A lightweight coil was designed to create minimum weight on UV. Electromagnetic interference (EMI) was kept low with the core in the designed coil structure. Therefore, it has become more beneficial for both UV and the environment. The design does not create an unbalanced load on the UV, has a minimum weight, and has low magnetic interference (by the standards). WPT circuit analyzes were performed on MATLAB/Simulink and ANSYS Simplorer. Coil design was carried out in ANSYS Maxwell 3D using FEM. On average, it was operated with a charging power of 3.3 kW and an efficiency of 92 % over a 10 cm air gap. In addition, its effect on human and living organism health was examined through the HFSS program.

[1] Electric-Electronic Engineering Department, Suleyman Demirel University, Isparta, Turkey, aliagcal@sdu.edu.tr
[2] Electric and Energy Department, Yatağan Vocational School, Muğla Sıtkı Koçman University, Muğla, Turkey, altankalay@mu.edu.tr
[3] Electric-Electronic Engineering Department, Suleyman Demirel University, Isparta, Turkey, cetinramazan306@gmail.com

2. MAGNETIC RESONANCE COUPLING THEORY

In the MRC theory-based WPT system, energy is transferred using coils by magnetic coupling between coils. The time-varying current flowing through the transmitter coil produces the time-varying magnetic field. The generated magnetic field induces a voltage in the receiving coil. High frequency makes the mutual impedance between the two coils high. Increasing the frequency reduces most of the power loss from loose coupling and increases efficiency. Also, unlike the classical magnetic induction system, the MRC system has a compensation structure using capacitors. In the WPT system using magnetic resonance coupling theory, the resonant frequency is captured at the maximum point of the energy flow between the receiver and transmitter. The maximum point of efficiency is obtained at this captured frequency. Figure 2 shows the MRC circuit with SS topology.

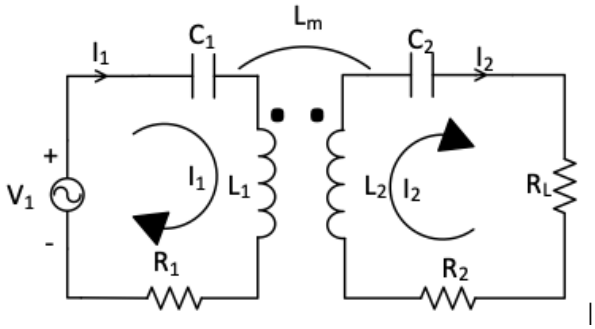

Fig. 2 – MRC circuit with SS topology.

In the equivalent circuit, I_1 input current (transmitter current), I_2 output current (receiver current), V_1 input voltage, and R_1 and R_2 transmitter and receiver systems' internal resistances. C_1 and C_2 are transmitter and receiver resonant capacitors, respectively. L_1 transmitter coil inductance, L_2 receive coil inductance, L_m mutual inductance, and Z_{load} (Z_0) indicate the load impedance (characteristic impedance). R_L is the load resistance. The natural angular resonance frequency ω_0 of the resonator and the quality factor (Q) are

$$\omega_o = \frac{1}{\sqrt{L\,C}}, \tag{1}$$

$$Q = \sqrt{\frac{L}{C}} x \frac{1}{R} = \frac{\omega_o L}{R}. \tag{2}$$

In WPT systems, the magnetic connection between the transmitting and receiving coils is provided by mutual inductance [15]. The ratio of the magnetic coupling is determined by proportioning the mutual inductance and the geometric mean of the inductances of the transmitter and receiver coils. The coupling factor is denoted by *k*. The relationship between the coupling factor and the mutual inductance is given in equation (3).

$$L_m = k\sqrt{L_1\,L_2}. \tag{3}$$

The critical mutual inductance value is calculated by [16]

$$L^2_{mcritical} = \frac{Z_0^2 - R^2}{\omega_0^2}. \tag{4}$$

If L_m is under the critical mutual inductance, the efficiency of the WPT system is below the maximum efficiency. If L_m is above the critical mutual inductance, The WPT is provided with high efficiency, but; resonant frequency bifurcates [6,15]. The equivalent impedance of the WPT circuit with SS topology in Fig. 2 is given in equation (5) and efficiency in equation (6).

$$Z_{Eq} = R_1 + j\omega L_1 + \frac{1}{j\omega C_1} + \left(\frac{{L_m}^2\omega^2}{R_2 + j\omega L_2 + \left(\frac{1}{j\omega C_2}\right) + R_L}\right) \tag{5}$$

$$\eta = \frac{P_{out}}{P_{in}} = \left|\left(\frac{jL_m\omega}{R_2 + j\omega L_2 + \left(\frac{1}{j\omega C_2}\right) + R_L}\right)^2 * \frac{R_L}{Z_{Eq}}\right| \tag{6}$$

where efficiency is calculated as the ratio of output active power (P_{out}) to input active power (P_{in}). In UV wireless applications, eddy currents occur in the water. For modelling the eddy current loss, resistors modelling the eddy current losses are added to the equivalent circuit in Fig. 2 [17]. An equivalent circuit with added resistors modelling eddy losses is shown in Fig. 3.

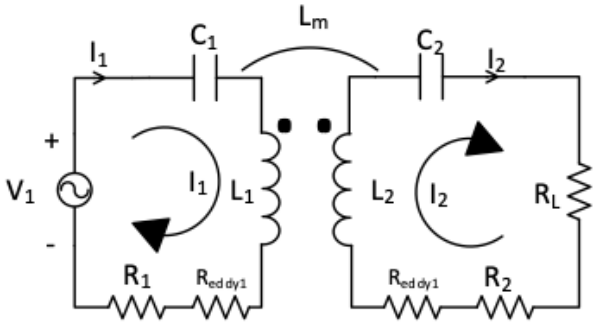

Fig. 3 – MRC circuit with eddy resistor attached with SS topology

R_{eddy1} and R_{eddy2} are the resistances of the eddy current losses acting on the transmitter and receiver coils, respectively. In the air and distilled water, it is R_{eddy}=0. The circuit equation of the circuit in Fig. 3 is shown in equation (7) and equation (8).

$$\bar{V}_1 = \left(R_1 + R_{eddy_1} + j\omega L_1 + \frac{1}{j\omega C_1}\right)\bar{I}_1 - (j\omega L_m)\bar{I}_2 \tag{7}$$

$$0 = -(j\omega L_m)\bar{I}_1 + \left(R_2 + R_L + R_{eddy_2} + j\omega L_2 + \frac{1}{j\omega C_2}\right)\bar{I}_2 \tag{8}$$

The equations of R_{eddy1} (9) and R_{eddy2} (10) are obtained by using equations (7) and (8).

$$R_{eddy_1} = \left|\frac{\bar{V}_1 + j\omega L_m \bar{I}_2}{\bar{I}_1} - R_1 - j\omega L_1 - \frac{1}{j\omega C_1}\right| \tag{9}$$

$$R_{eddy_2} = \left|\frac{j\omega L_m \bar{I}_1}{\bar{I}_2} - R_2 - R_L - j\omega L_2 - \frac{1}{j\omega C_2}\right| \tag{10}$$

For calculating R_{eddy1} and R_{eddy2}, information on V_1, I_1 and I_2 are obtained from experiments or simulation. In equations (9) and (10), attention should be paid to the amplitude and phase angle of the measured V_1, I_1, and I_2.

2.1. SQUARE COIL DESIGN

A planar spiral square coil is shown in Fig. 4. In a square coil, N is the number of turns, D_{out} is the outer edge length, w is the conductor diameter, and s is the space between conductors. Length units are in meters. In [18], different methods have been proposed for the self-inductance of a planar square coil. The first is the modified Wheeler formula

for flat spiral inductors. The modified Wheeler formula for the planar spiral square coil is illustrated by

$$L_{Wheeler} = 2.34\mu_0 \frac{N^2 d_{avg}}{1+2.75\rho} \quad (11)$$

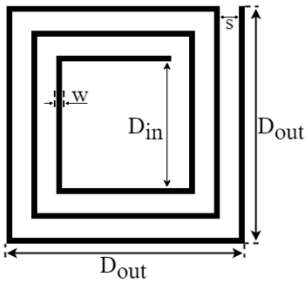

Fig. 4 – Spiral square coil

The value of the magnetic permeability μ_0 (vacuum permeability) is 4π x 10^{-7} H/m. d_{avg} is the mean diameter calculated by equation (12), and ρ is the filling ratio by

$$d_{avg} = \frac{d_{out}+d_{in}}{2} \quad (12)$$

$$\rho = \frac{d_{out}-d_{in}}{d_{out}+d_{in}} \quad (13)$$

$$D_{in} = D_{out} - 2N(s+w) + 2s \quad (14)$$

d_{in} is the inner edge length. Another formula is derived from electromagnetic principles. The so-called 'Expression Based on Current Sheet Approximation' formula for the inductance of a flat spiral can be obtained by approximating the edges of the spirals with symmetrical current sheets with equal current densities. In the square case, there are four identical current plates. Existing plates on opposite sides are parallel, while adjacent ones are perpendicular. It exploits the symmetry and the fact that the vertical plates have zero mutual inductance. The calculation of inductance is reduced to evaluating the self-inductance of a plate and the mutual inductance between the reverse current plates. As a result, the expression for the square coil is given by (15) [18].

$$L_{CS} = \frac{1.27\mu_0 N^2 d_{avg}}{2}\left(\ln\left(\frac{2.07}{\rho}\right) + 0.18\rho + 0.13\rho^2\right) \quad (15)$$

The planar square coil conductor length is calculated by

$$l_{square} = \sum_{i=1}^{4N} l_i \quad (16)$$

$$l_i = D_{out} - < \frac{i}{2} - 1 > (w+s) \quad (17)$$

l_{square} is the total wire length. l_i is the length of each piece of wire. i for the square coil in Figure 4 is obtained by numbering from the outside to the inside (1,2, 3, ...). Four pieces of wire are on each edge, so there are 4N pieces of wire for N turns. < > denotes the integer part of the number in brackets [19].

3. UNDERWATER WPT SYSTEM DESIGN

A WPT system with an operating frequency of 85 kHz, power of 3.3 kW, and a coil size of 50 cm – 50 cm was designed. The design used square coils with a conductor diameter of 3.1 mm, a distance between conductors of 0.5 mm, 9 turns of 9, an inner edge length of 443.7 mm, and an outer edge length of 500 mm for the receiver and transmitter. The design has been tested in air, seawater, and distilled water. Fig. 5 shows the coils designed in Maxwell 3D.

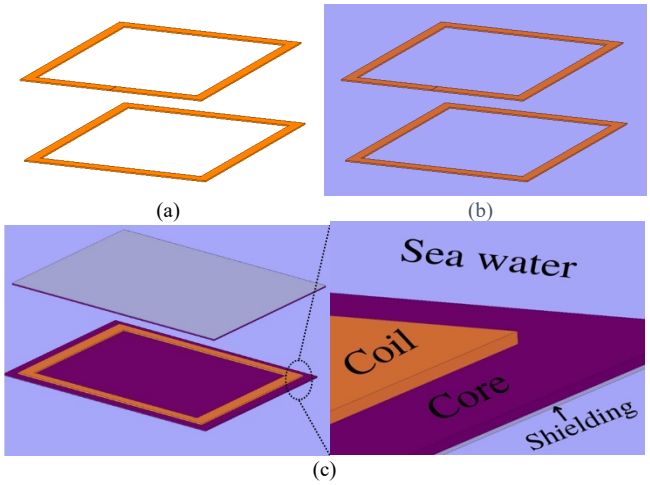

Fig. 5 – Coil design in (a) air, (b) seawater(coreless) and (c) seawater (core and shielded)

The self-inductance of the designed coil was calculated by current sheet method, modified Wheeler formula and the Maxwell 3D. Circuit parameters of the designed WPT are given in Table 1.

Table 1

Circuit parameters for air, seawater and distilled water environment

Air	Distilled Water	Sea Water without core and shielding	Sea Water with core and shielding
$C_1 = C_2$= 35.1 nF	$C_1 = C_2$= 35.1 nF	$C_1 = C_2$= 35.1 nF	$C_1 = C_2$= 35.1 nF
$L_1 = L_2$= 105.88 µ*H (Maxwell 3D)* $L_1 = L_2$= 108.3 µ*H (Current Sheet)* $L_1 = L_2$= 96.44 µ*H (Mod. Wheeler)*	$L_1 = L_2$= *105.88 µH (Maxwell 3D)* $L_1 = L_2$= 108.3 µ*H (Current Sheet)* $L_1 = L_2$= 96.44 µ*H (Mod. Wheeler)*	$L_1 = L_2$= 104.98 µH *(Maxwell 3D)* $L_1 = L_2$= 108.3 µ*H (Current Sheet)* $L_1 = L_2$= 96.44 µ*H (Mod. Wheeler)*	$L_1 = L_2$= 105.71 µH *(Maxwell 3D)*
Wire length 17.09 m	Wire length 17.09 m	Wire length 17.09 m	Wire length 13.38 m
$R_1 = R_2$ = 0.097 Ω	$R_1 = R_2$ =0.097 Ω	$R_1 = R_2$ = 0.097 Ω	$R_1 = R_2$ = 0.076 Ω
L_{m10}= 29.13 µ*H (*10 cm air gap*)*	L_{m10}= 29.13 µ*H (*10 cm air gap*)*	L_{m10}= 28.82 µ*H (*10 cm air gap*)*	L_{m10}= 31.46 µ*H (*10 cm air gap*)*
L_{m30}= 8.4 µ*H (*30 cm air gap*)*	L_{m30}= 8.4 µ*H (*30 cm air gap*)*	L_{m30}= 8.12 µ*H (*30 cm air gap*)*	L_{m30}= 6.66 µ*H (*30 cm air gap*)*

The eddy current losses of the coreless and unshielded system were high; to reduce these losses, it was necessary to limit the magnetic flux paths except for the regions between the receiver and the transmitter. For this reason, a cored and shielded system has been designed. Ferrite cores are placed behind the magnetic coils and are used to increase mutual inductance and reduce leakage fluxes and magnetic reluctance. However, the ferrite core is insufficient to limit the high magnetic field interference and an additional shielding element is needed. Therefore, the other side of the ferrite core

is covered with an aluminum shield. Aluminum is a diamagnetic material. Leakage magnetic flux lines create eddy currents on aluminum. Thus, the magnetic field interference cannot pass through the aluminum, and the device behind the aluminum is protected [20]. The core and aluminum shielding are dimensions 500 mm x 500 mm x 2.5 mm and 500 mm x 500 mm x 0.1 mm, respectively. The cored and shielded coil is wound as 7 turns for the inductance value of the coreless and shieldless coil design to be the same as the cored and shielded coil.

The core is placed between the aluminum shielding and the coil and in contact with both structures without gaps. In the study, coreless unshielded coils and coreless and shielded coils were simulated at different frequencies. The conductivity of seawater is taken at 4 S/m. The R_{eddy} is calculated using the simulation results, eq. (9), and eq. (10). The variation of R_{eddy} resistance according to the frequency in the seawater environment is given in Fig. 6.

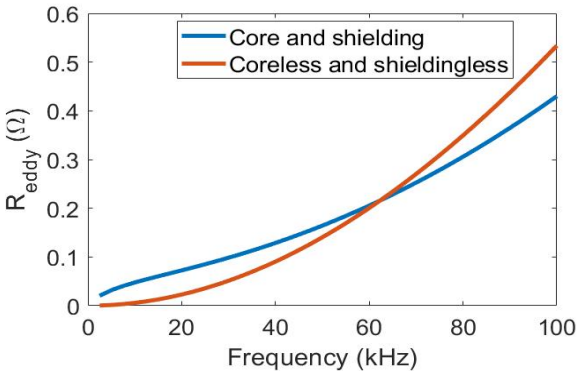

Fig. 6 – Variation of R_{eddy} resistance with frequency in seawater environment

The analytical solution of the circuit was made in MATLAB/Editor. WPT system was analyzed by load resistance R_L = 5 Ω set up for 10 cm and 30 cm air gaps. A single resonance situation occurs in the WPT system with SS topology if the L_m is below the $L_{mcritical}$ (Equation 4). The variation of efficiency and equivalent impedance according to the frequency in air and distilled water, seawater without core and shielding, and seawater with core and shielding for a 30 cm air gap is shown in Fig. 7.

η_{ADW} is the efficiency of air and distilled water, η_{Sea} is the efficiency of seawater without core and shielding, and η_{SCS} is the efficiency of seawater with core and shielding. Respectively, $Z_{Eq_{ADW}}$, $Z_{Eq_{Sea}}$, and, $Z_{Eq_{SCS}}$ are equivalent impedance of the air and distilled water, seawater without core and shielding, and seawater with core and shielding. In the single resonant frequency situation, the efficiency at the resonant frequency is maximum, and the equivalent impedance is minimum. Three resonant states in the WPT system with SS topology occur if the L_m is above the $L_{mcritical}$ (eq. 4).

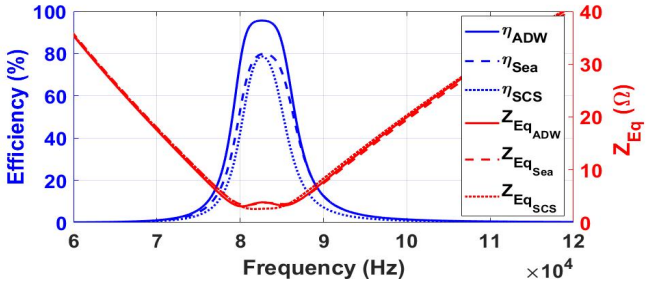

Fig. 7 – Efficiency-frequency and equivalent impedance-frequency graph for 30 cm air gap

The variation of efficiency and equivalent impedance according to frequency for the 10 cm air gap is shown in Fig. 8.

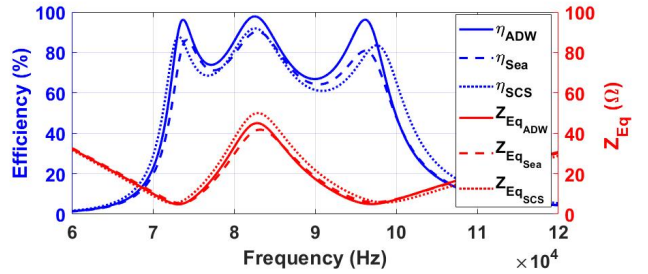

Fig. 8 – Efficiency-frequency and equivalent impedance-frequency plot for 10 cm air gap

It is seen in Table 1 that L_m for a 10 cm air gap is greater than $L_{mcritical}$. Therefore, it is seen in Fig. 8 that three resonant frequencies occur. At the first and third resonance frequencies, Z_{Eq} was minimum, and efficiency was maximum. However, Z_{Eq} at the second resonance frequency is higher than the first resonance and third resonance frequencies. In the case of bifurcation, as the air gap decreases, the Z_{Eq} value at the second resonance frequency increases and the power drawn from the input decreases. Therefore, operating at the second resonance frequency in WPT systems with SS topology was not preferred. In the studies, the first resonance frequency with the lowest frequency was preferred to avoid increasing the AC resistances due to the skin and proximity effects. In addition, the first resonance frequency was preferred in studies since eddy current losses were directly proportional to the frequency in the seawater environment. The WPT circuit was created on MATLAB/Simulink, and the circuit simulation was carried out. Figure 9 shows the WPT System circuit modelled in MATLAB/Simulink.

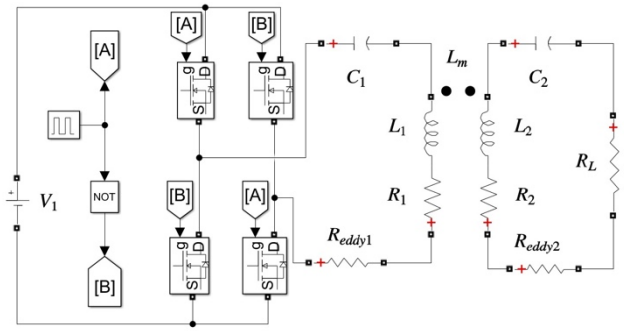

Fig. 9 – WPT System circuit modelled in Simulink.

In a seawater environment, coreless and unshielded coils and cored and shielded coils were simulated for 10 cm and 30 cm air gaps. Values from MATLAB Simulink are given

in Table 2. Table 2 shows that eddy current losses were reduced at close ranges using core and shielding in submarine WPT applications. At long distances, the coupling factor of the cored and shielded system is lower than the coreless and unshielded systems. Therefore, a coreless unshielded system is more suitable for long distances. However, since the submarine hull provides the shielding, a design without shielding is impossible in practical applications. Since using only a shielded system greatly reduces efficiency, a cored and shielded system is preferred.

Table 2.
MATLAB-Simulink Results

Air gap = 30 cm		Air gap = 10 cm	
Coreless and shieldless coils	Coils with core and shielding	Coreless and shieldless coils	Coils with core and shielding
L_m = 8.12 µH	L_m = 6.66 µH	L_m = 28.82 µH	L_m = 31.46 µH
f_r = 82920 Hz	f_r = 82650 Hz	f_r = 82890 Hz	f_r = 82590 Hz
Z_{Eq} = 3.742 Ω	Z_{Eq} = 2.612 Ω	Z_{Eq} = 41.65 Ω	Z_{Eq} = 49.79 Ω
η = 80.36 %	η = 78.98 %	η = 90.78 %	η = 92.34 %
$V_{1(avg)}$ = 139.3 V	$V_{1(avg)}$ = 118 V	$V_{1(avg)}$ = 432.8 V	$V_{1(avg)}$ = 469.5 V
$V_{2(rms)}$ = 128.4 V	$V_{2(rms)}$ = 128.6 V	$V_{2(rms)}$ = 128.4 V	$V_{2(rms)}$ = 128.6 V
$I_{1(rms)}$ = 33.21 A	$I_{1(rms)}$ = 40.06 A	$I_{1(rms)}$ = 9.42 A	$I_{1(rms)}$ = 8.55 A
$I_{2(rms)}$ = 25.68 A	$I_{2(rms)}$ = 25.71 A	$I_{2(rms)}$ = 25.68 A	$I_{2(rms)}$ = 25.72 A
$P_{1(rms)}$ = 4109 W	$P_{1(rms)}$ = 4182 W	$P_{1(rms)}$ = 3635 W	$P_{1(rms)}$ = 3575 W
$P_{2(rms)}$ = 3302 W	$P_{2(rms)}$ = 3303 W	$P_{2(rms)}$ = 3300 W	$P_{2(rms)}$ = 3301 W
$V_{C1(rms)}$ = 1812 V	$V_{C1(rms)}$ = 2197 V	$V_{C1(rms)}$ = 511.6 V	$V_{C1(rms)}$ = 465.9 V
$V_{C2(rms)}$ = 1403 V	$V_{C2(rms)}$ = 1407 V	$V_{C2(rms)}$ = 1403 V	$V_{C2(rms)}$ = 1408 V

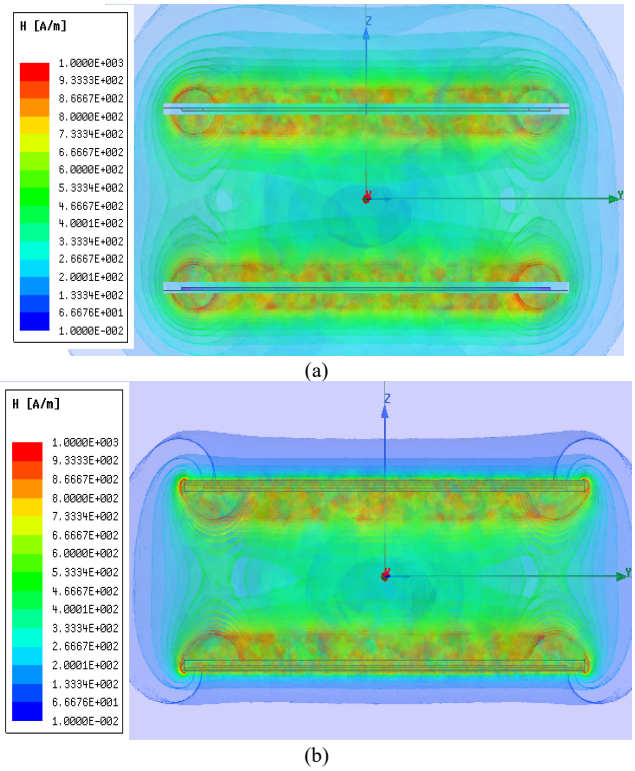

Fig. 10 – (a) Unshielded and coreless and (b) core and shielded magnetic field

It was observed that the magnetic field spreads as in Fig. 10(a) without shielding. A shielding system is placed behind the coil to prevent this spread. The shielding and core structure ensure that the magnetic field remains between the receiver and the transmitter coil, as in Fig. 10(b). Thus, the area where the living things in the environment are affected by the magnetic field is minimized.

During wireless energy transfer under the sea, the magnetic field values between the receiver and transmitter may be above the limit values. Fig. 11 shows the magnetic flux distribution on a line drawn on the horizontal axis from the middle of the coils.

On the horizontal axis, it can be seen from Fig. 11 that the cored system is 52 cm away from the center, and the coreless system is 62 cm away from the center, falling below 27 µT. It is seen that it is necessary to turn off the WPT system when a living thing comes within 52 cm of the receiver or transmitter in the core and shielded system not to harm the living things.

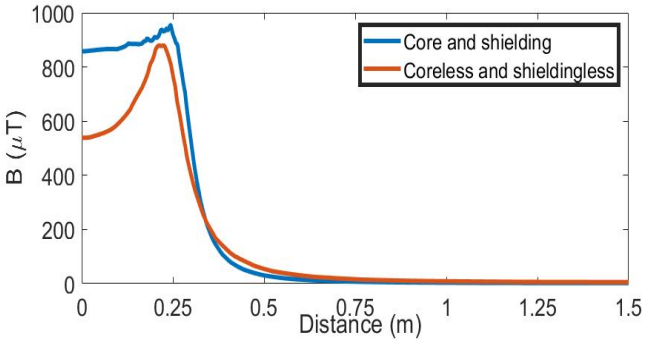

Fig. 11 – Magnetic flux density on the horizontal axis

Based on IEEE standards [21] and ICNIRP guidelines [22], it has been observed that the WPT design is not harmful to human health for distances of 52 cm and above.

4. CONCLUSIONS

Wired transmission of power to electric vehicles operating underwater poses a danger due to the corrosion of underwater cables and the conductivity of seawater. WPT provides a reliable and autonomous solution for the charging of UV. This study investigated WPT systems in different environments, such as air, distilled water, and seawater. The effects of seawater on the WPT system were analyzed, and eddy current losses in seawater were modelled. A WPT

system with 85 kHz frequency and a power of 3.3 kW was analyzed in various environments between 10 cm and 30 cm.

This modelling proposed a coil design that reduces seawater's eddy current losses and magnetic scattering. Above the critical mutual inductance, core and shielding reduce magnetic scattering and seawater's eddy current losses. However, below the critical mutual inductance, since the number of turns of the coil with the core is lower than the coreless coil, its magnetic coupling is lower at long distances. Therefore, below the critical mutual inductance, the loss of the coil with the core is higher than the coreless coil at the same inductance value. While the WPT system works with high efficiency in air and pure water, it was observed to work with a bit lower efficiency in a seawater environment due to eddy current losses. In addition, the magnetic field and magnetic flux densities created by the transmitter and receiver coils were investigated by using the ANSYS Maxwell 3D program. When living or inanimate objects come within 52 cm of the coils, the WPT system must be turned off to protect living things and themselves using an object detection system.

ACKNOWLEDGMENT

This research is funded by the Süleyman Demirel University Scientific Research Projects Coordination Unit under project number FYL-2022-8681.

Received on 10 November 2022

REFERENCES

1. C. Cai, Y. Zhang, S. Wu, J. Liu, Z. Zhang, L. Jiang, *A circumferential coupled dipole-coil magnetic coupler for autonomous underwater vehicles wireless charging applications*, IEEE Access, **8**, pp. 65432-65442 (2020).
2. X. Lu, P. Wang, D. Niyato, D.I. Kim, Z. Han, *Wireless charging technologies: Fundamentals, standards, and network applications*, IEEE Communications Surveys & Tutorials, **18**, *2*, pp. 1413-1452 (2015).
3. J. Kim, K. Kim, H. Kim, D. Kim, J. Park, S. Ahn, *An efficient modeling for underwater wireless power transfer using Z-parameters.* IEEE Transactions on Electromagnetic Compatibility, **61**, *6*, pp. 2006-2014 (2019).
4. J. Garnica, R. A. Chinga, & J. Lin, *Wireless power transmission: From far field to near field,* Proc. of the IEEE, **101**, *6*, pp. 1321-1331 (2013).
5. Z. Liu, L. Wang, Y. Guo, C. Tao, *Eddy current loss analysis of wireless power transfer system for autonomous underwater vehicles*, In 2020 IEEE PELS Workshop on Emerging Technologies: Wireless Power Transfer (WoW), pp. 283-287 (2020).
6. A. Agcal, S. O. Ozkilic, K. Toraman, *Comparison of compensating topologies in two coils resonant wireless power transfer system*. Journal of Engineering Research (2022).
7. C.R. Teeneti, T.T. Truscott, D.N. Beal, Z. Pantic, *Review of wireless charging systems for autonomous underwater vehicles.* IEEE Journal of Oceanic Engineering, **46**, *1*, pp. 68-87 (2019).
8. L. Yang, M. Ju & B. Zhang, *Bidirectional undersea capacitive wireless power transfer system.* IEEE Access, **7**, pp. 121046-121054 (2019).
9. L. Yang, Y. Zhang, X. Li, J. Jian, Z. Wang, J. Huang, X. Tong, *Analysis and design of four-plate capacitive wireless power transfer system for undersea applications.* CES Transactions on Electrical Machines and Systems, **5**,*3*, pp. 202-211(2021).
10. K. Zhang, X. Zhang, Z. Zhu, Z. Yan, B. Song, C.C.Mi, *A new coil structure to reduce eddy current loss of WPT systems for underwater vehicles*. IEEE Transactions on Vehicular Technology, **68**, *1*, pp. 245-253 (2018).
11. M. Ogihara, T. Ebihara, K. Mizutani, N. Wakatsuki, *Wireless power and data transfer system for station-based autonomous underwater vehicles.* In *OCEANS 2015-MTS/IEEE Washington*, pp. 1-5 (2015).
12. D. Wang, S. Cui, J. Zhang, Z. Bie, K. Song, C. Zhu, *A novel arc-shaped lightweight magnetic coupler for AUV wireless power transfer*, IEEE Transactions on Industry Applications, **58**, *1*, pp. 1315-1329 (2022).
13. T. Kan, R. Mai, P.P. Mercier, C.C. Mi, *Design and analysis of a three-phase wireless charging system for lightweight autonomous underwater vehicles*, IEEE Transactions on power electronics, **33**, *8*, pp. 6622-6632 (2017).
14. Y. Zeng, C. Rong, C. Lu, X. Tao, X. Liu, R. Liu, M. Liu, *Misalignment insensitive wireless power transfer system using a hybrid transmitter for autonomous underwater vehicles.* IEEE Transactions on Industry Applications, **58,** *1*, pp. 1298-1306 (2022).
15. A. Agcal, S. Ozcira, N. Bekiroglu, *Wireless power transfer by using magnetically coupled resonators*. Journal of Wireless Power Transfer: Fundamentals and Technologies, pp. 49-66 (2016).
16. T. Imura, Y. Hori, *Maximizing air gap and efficiency of magnetic resonant coupling for wireless power transfer using equivalent circuit and Neumann formula*. IEEE Trans. Ind. Electron, **58**, *10*, pp. 4746–4752 (2011).
17. W. Niu, C. Ye, W. Gu, *circuit coupling model containing equivalent eddy current loss impedance for wireless power transfer in seawater,* **15**, pp. 410-416 (2021).
18. S.S. Mohan, M. del Mar Hershenson, S.P. Boyd, T.H. Lee, *Simple accurate expressions for planar spiral inductances,* IEEE Journal of solid-state circuits, **34**, *10*, pp. 1419-1424 (1999).
19. Z. Duan, Y. X. Guo, D. L. Kwong, *Rectangular coils optimization for wireless power transmission*. Radio Science, **47**, *3*, pp. 1-10 (2012).
20. Kim, Jiseong et al., *Coil design and shielding methods for a magnetic resonant wireless power transfer system*. Proceedings of the IEEE, **101**, *6*, pp. 1332-1342 (2013).
21. ***IEEE, *Standard for safety levels with respect to human exposure to electric, magnetic, and electromagnetic fields (0 Hz to 100 kHz)* (2019).
22. ***International Commission on Non-Ionizing Radiation Protection (ICNIRP), *Guidelines for limiting exposure to time-varying electric and magnetic fields for low frequencies (1 Hz–100 kHz). Health Phys*. Internatıonal Commission on Non-Ionizing Radiation Protection (2010).